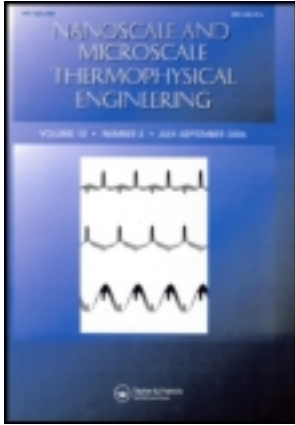


This article was downloaded by: [Purdue University]

On: 19 April 2014, At: 11:24

Publisher: Taylor & Francis

Informa Ltd Registered in England and Wales Registered Number: 1072954 Registered office: Mortimer House, 37-41 Mortimer Street, London W1T 3JH, UK



Nanoscale and Microscale Thermophysical Engineering

Publication details, including instructions for authors and subscription information:

<http://www.tandfonline.com/loi/umte20>

Measurement of In-Plane Thermal Conductivity of Ultrathin Films Using Micro-Raman Spectroscopy

Zhe Luo^a, Han Liu^b, Bryan T. Spann^a, Yanhui Feng^c, Peide Ye^b, Yong P. Chen^d & Xianfan Xu^a

^a School of Mechanical Engineering and Birck Nanotechnology Center, Purdue University, West Lafayette, Indiana

^b School of Electrical and Computer Engineering and Birck Nanotechnology Center, Purdue University, West Lafayette, Indiana

^c School of Mechanical Engineering, University of Science and Technology Beijing, Beijing, China

^d Department of Physics and Birck Nanotechnology Center, Purdue University, West Lafayette, Indiana

Published online: 14 Apr 2014.

To cite this article: Zhe Luo, Han Liu, Bryan T. Spann, Yanhui Feng, Peide Ye, Yong P. Chen & Xianfan Xu (2014) Measurement of In-Plane Thermal Conductivity of Ultrathin Films Using Micro-Raman Spectroscopy, *Nanoscale and Microscale Thermophysical Engineering*, 18:2, 183-193, DOI: [10.1080/15567265.2014.892553](https://doi.org/10.1080/15567265.2014.892553)

To link to this article: <http://dx.doi.org/10.1080/15567265.2014.892553>

PLEASE SCROLL DOWN FOR ARTICLE

Taylor & Francis makes every effort to ensure the accuracy of all the information (the "Content") contained in the publications on our platform. However, Taylor & Francis, our agents, and our licensors make no representations or warranties whatsoever as to the accuracy, completeness, or suitability for any purpose of the Content. Any opinions and views expressed in this publication are the opinions and views of the authors, and are not the views of or endorsed by Taylor & Francis. The accuracy of the Content should not be relied upon and should be independently verified with primary sources of information. Taylor and Francis shall not be liable for any losses, actions, claims, proceedings, demands, costs, expenses, damages, and other liabilities whatsoever or howsoever caused arising directly or indirectly in connection with, in relation to or arising out of the use of the Content.

This article may be used for research, teaching, and private study purposes. Any substantial or systematic reproduction, redistribution, reselling, loan, sub-licensing, systematic supply, or distribution in any form to anyone is expressly forbidden. Terms & Conditions of access and use can be found at <http://www.tandfonline.com/page/terms-and-conditions>

MEASUREMENT OF IN-PLANE THERMAL CONDUCTIVITY OF ULTRATHIN FILMS USING MICRO-RAMAN SPECTROSCOPY

Zhe Luo¹, Han Liu², Bryan T. Spann¹, Yanhui Feng³, Peide Ye², Yong P. Chen⁴, and Xianfan Xu¹

¹*School of Mechanical Engineering and Birck Nanotechnology Center, Purdue University, West Lafayette, Indiana*

²*School of Electrical and Computer Engineering and Birck Nanotechnology Center, Purdue University, West Lafayette, Indiana*

³*School of Mechanical Engineering, University of Science and Technology Beijing, Beijing, China*

⁴*Department of Physics and Birck Nanotechnology Center, Purdue University, West Lafayette, Indiana*

We report a micro-Raman-based optical method to measure in-plane thermal conductivity of ultrathin films. With the use of 20-nm-thick SiO₂ substrates that assure in-plane heat transfer, sub-100-nm Bi films and Al₂O₃ films as thin as 5 nm were successfully measured. The results of Bi films reveal that phonon boundary scattering, both at the surface/interface and at the grain boundaries, reduces in-plane lattice thermal conductivity. The measurements of amorphous Al₂O₃ films were accomplished using thin Bi film as a Raman temperature sensor, and the results agree with the minimum thermal conductivity models for dielectrics. Our work demonstrates that the micro-Raman method is promising for characterization of in-plane thermal conductivity and phonon behaviors of thin-film structures if the Raman temperature sensor material and substrate material are carefully selected.

KEY WORDS: micro-Raman, in-plane thermal conductivity, thin films, phonon boundary scattering

INTRODUCTION

In the past decades, thermal transport in thin-film structures has been extensively studied for applications such as thermal management in electronic devices [1, 2] and thin-film thermoelectrics [3–6]. Thin-film boundaries and interfaces contain roughness and defects that can scatter phonons efficiently [7, 8] and reduce the lattice thermal conductivity, which is advantageous for thermoelectrics to increase the thermoelectric figure of merit $ZT = \sigma S^2 T/k$, where σ is the electrical conductivity, S is the Seebeck coefficient, T is the absolute temperature, and k is the thermal conductivity. On the other hand, suppressed thermal conductivity in nanoscale semiconducting or dielectric films reduces the

Manuscript received 23 August 2013; accepted 5 February 2014.

Address correspondence to Xianfan Xu, School of Mechanical Engineering, Purdue University, 585 Purdue Mall, West Lafayette, IN 47907. E-mail: xxu@ecn.purdue.edu

Color versions of one or more of the figures in the article can be found online at www.tandfonline.com/umte.

heat removal efficiency in electronic devices whose power density increases at the pace predicted by Moore's law. Therefore, it is crucial to characterize the thermal conductivity of thin-film-based devices to both evaluate their performance and reveal the underpinning physical nature of heat transport.

Much effort has been devoted to measuring thin-film thermal conductivity. To measure the cross-plane thermal conductivity, the 3ω method [9–12] and the time-domain thermorefectance method [13–15] have been widely used. These are well-developed techniques but are mostly limited to the measurement of cross-plane thermal conductivity, because the characteristic size of the heat source (metal heater or focused laser spot) is usually larger than the film thickness so that the cross-plane heat transfer into the underneath layers or substrate is dominant. The thin-film in-plane thermal conductivity measurement remains difficult [5] because the unfavorable heat flow into the substrate narrows the choice of the substrate material and the measureable film thickness, usually to hundreds of nanometers. The reported techniques include steady-state or transient (3ω) heater wire method on suspended film [16] and microfabricated heater bridge [17]. Most of these methods require very careful sample preparation and handling and sometimes complicated modeling due to the irregular geometry involving additional structures such as a heater.

In this work, we describe a noncontact, micro-Raman spectroscopy-based technique that can potentially be applied to the in-plane thermal conductivity measurement of thin films with sub-100-nm thickness. Micro-Raman systems tightly focus a laser beam on the sample and collect the scattered photons whose frequency changes by a certain amount due to photon–phonon inelastic scattering with the sample molecules or the periodic lattice structure, which is known as Raman scattering. In our work, the same laser also induces a heating effect, shifting the Raman peak due to bond softening and thermal expansion. Temperature information can be obtained by measuring this heat-induced Raman peak shift. Using a simple heat transfer model, the in-plane thermal conductivity of the sample can be extracted. To ensure that the heat transfer is in-plane dominated and can be neglected in the cross-plane direction, the in-plane dimension should be much larger than the cross-plane dimension of the film. In terms of measuring in-plane thermal conductivity of thin films, the micro-Raman method has been applied to a limited degree to mechanically exfoliated 2D films such as single-layer graphene [18–21] (thickness ~ 0.35 nm). In this work, we measured sub-100-nm-thick Bi films and used Bi films as Raman transducers to measure Al_2O_3 films. SiO_2 membranes with a 20-nm thickness were used as substrates. This allows a selection of various types of thin-film materials to be measured while still maintaining a very small total film thickness comparing with the lateral dimension. The low thermal conductivity of SiO_2 ($k = 1.4$ W/mK [22]) minimizes the parasitic in-plane heat flow in the substrate, which enhances the measurement sensitivity.

EXPERIMENTS AND MODELING

Sample Preparation

The thin-film substrates used were 20-nm-thick, $100\ \mu\text{m} \times 100\ \mu\text{m}$ SiO_2 membranes suspended on Si frames. The membranes were pure stoichiometric SiO_2 prepared by sputtering from an SiO_2 target in an oxygen atmosphere. To measure the in-plane thermal conductivity of Bi films, polycrystalline Bi films of thickness ranging from 20 to 145 nm were thermally evaporated on the SiO_2 substrates with a vacuum pressure $< 10^{-6}$ Torr. The

Raman shift in Bi produced by laser heating was used as the temperature sensor. To measure the in-plane thermal conductivity of thin Al₂O₃ films, 5- to 30-nm-thick Al₂O₃ films were deposited on the same SiO₂ membranes by atomic layer deposition (ALD) and then coated with 20-nm-thick Bi films as the Raman temperature sensors because ALD-prepared Al₂O₃ was amorphous and did not show Raman peaks. During each deposition process, a glass substrate was coated simultaneously as a reference to measure the actual film thickness by performing atomic force microscope scans after intentionally scratching the reference thin-film sample.

Micro-Raman Measurement Method

The experimental setup is illustrated in [Figure 1a](#). A 632.8-nm HeNe laser was focused by an Olympus 50× objective (MPLN50x, Olympus America) at the center of the sample placed in an open air environment at room temperature. This configuration suggests a temperature distribution profile that is axisymmetric in the radial direction and uniform in the vertical direction, because the film thickness is much smaller than its radial dimension. The excited Raman scattering was collected by a HORIBA LabRAM HR800 Raman spectrometer (HORIBA Jobin Yvon, NJ, USA). The instrument has a spectral uncertainty of 0.27 cm⁻¹ and peak fitting uncertainty of 0.02–0.07 cm⁻¹. A power meter was placed under the sample to measure the optical transmissivity T . At the entrance of the Raman microscope, a beam splitter was used to direct the reflected light from the sample into a power meter; by using a metallic mirror reference we obtained the reflectivity R of the sample. A variable neutral density filter tuned the input laser power to change the sample temperature and subsequently changed the Raman peak shift. With a calibration process, the Raman peak shifts were interpreted to the temperature variations, which were then used to model the heat transfer process.

The laser spot radius r_0 is a critical parameter for the in-plane thermal conductivity calculation. To obtain r_0 , a knife-edge measurement based on Raman intensity was performed using a sharp Si sample. A piezo-electric stage drove the Si edge to pass through the focused laser beam, and the intensity of the Si Raman peak at 520 cm⁻¹ was recorded as a function of the stage position. Raman scattering intensity is proportional to the incident laser power, so the Raman intensity as a function of stage position can be written as an integral of the Gaussian laser intensity profile and fitted by a complementary error function:

$$\Phi(x) = \int_{-\infty}^{\infty} \int_{-\infty}^{x-x_0} I_0 \exp\left(-\frac{x'^2 + y'^2}{r_0^2}\right) dx' dy' = C \left[1 - \frac{1}{2} \operatorname{erfc}\left(\frac{x-x_0}{r_0}\right)\right]. \quad (1)$$

[Figure 1c](#) shows the data and fitting result. It yields a laser focal spot radius $r_0 = 500 \pm 33$ nm.

Heat Transfer Model

Under 1D assumption, the radial heat transfer equation for our thin-film laser heating problem is described as follows:

$$\frac{1}{r} \frac{d}{dr} \left(kr \frac{dT}{dr} \right) + \dot{q} = 0 \quad (2)$$

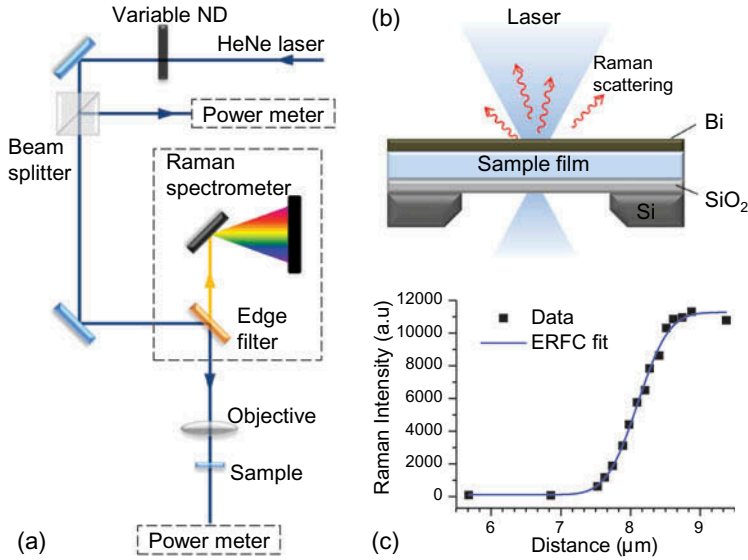


Figure 1 (a) Schematic of the experimental setup. (b) Schematic of the sample structure. The sample film is sandwiched between the Raman sensor Bi and the substrate SiO₂. The film stack lies on an Si frame. For the measurement of Bi films, there is no layer in between. (c) Laser spot size measurement results. The blue curve is the complementary error function fitting of the data.

The heat source term \dot{q} is attributed to the absorbed laser power in Bi film, which spreads as a Gaussian function along the in-plane direction and distributes uniformly in the cross-plane direction:

$$\dot{q} = \frac{1 - R - T}{t} \frac{P}{\pi r_0^2} \exp\left(-\frac{r^2}{r_0^2}\right), \quad (3)$$

where t is the total thickness of the sample film stack, P is the total laser power, and r_0 is the radius of the laser focal spot. Then the radial energy equation becomes

$$\frac{1}{r} \frac{d}{dr} \left(k_{eq} r \frac{dT}{dr} \right) + \frac{1 - R - T}{t} \frac{P}{\pi r_0^2} \exp\left(-\frac{r^2}{r_0^2}\right) = 0. \quad (4)$$

Here, k_{eq} stands for the equivalent in-plane thermal conductivity of the film stack:

$$k_{eq} = \frac{1}{t} \sum_{i=1}^n k_i t_i, \quad (5)$$

where k_i and t_i are the thermal conductivity and the thickness of the i th layer, respectively. At the edge of the film stack, the temperature is assumed equal to the room temperature T_0 , because the supporting silicon frame has a much higher thermal conductivity (148 W/mK) than the film stack, thus acting as an efficient heat sink that immediately lowers the boundary temperature to the ambient level.

Because the experiments were performed in an open air environment, it is necessary to evaluate the contributions of convective and radiative heat transfer. We estimated the 48-nm Bi film sample with 100- μ W incident power. According to our numerical analysis, the area-weighted average temperature rise in the film is within 5 K, then the convective heat transfer $q_{\text{conv}} = 2hA(T_{\text{avg}} - T_0) = 2 \mu\text{W}$, where the convective heat transfer coefficient h is assumed to be 20 W/m²K and the sample area $A = 100 \times 100 \mu\text{m}^2$. In addition, assuming that the temperature rise mainly occurs within a circular region of 20 μm radius r , the radiative heat transfer can be estimated as $q_{\text{rad}} = 2\sigma\pi r^2(T_{\text{peak}}^4 - T_0^4) = 0.78 \mu\text{W}$, with the peak temperature $T_{\text{peak}} = 340$ K. It can be seen that both convective and radiative heat transfer are much smaller and thus are neglected compared to the total absorbed laser power on the order of 50 μ W. With convective and radiative heat transfer neglected, the temperature field can be solved from Eq. (4) as

$$T(r) = T_0 + \frac{(1 - R - T)P}{2\pi k_{\text{eq}}t} \left\{ \left[\frac{1}{2} \text{Ei} \left(-\frac{r^2}{r_0^2} \right) - \ln \frac{r}{r_0} \right] - \left[\frac{1}{2} \text{Ei} \left(-\frac{r_b^2}{r_0^2} \right) - \ln \frac{r_b}{r_0} \right] \right\}, \quad (6)$$

where $\text{Ei}(x)$ is the exponential integral, r_b is the equivalent radius of the square film, which is the square root of A/π , where A is the sample area. According to our numerical calculations using both circular and square sample geometries, the approximation of using circular geometry with equivalent radius resulted in less than 4% discrepancy in the deduced in-plane thermal conductivity.

The temperature measured by the Raman laser beam is the Gaussian-weighted average temperature:

$$T_{\text{Raman}} = \frac{\int_0^\infty T(r) \exp\left(-\frac{r^2}{r_0^2}\right) r dr}{\int_0^\infty \exp\left(-\frac{r^2}{r_0^2}\right) r dr}. \quad (7)$$

It can be shown that the Raman-measured temperature at the laser focal spot rises linearly with laser power, and the temperature rising rate is a function of the equivalent thermal conductivity of the sample film stack given in Eq. (5):

$$\begin{aligned} \frac{dT_{\text{Raman}}}{dP} &= \frac{1 - R - T}{2\pi k_{\text{eq}}t} \left\{ \frac{\int_0^\infty \left[\frac{1}{2} \text{Ei} \left(-\frac{r^2}{r_0^2} \right) - \ln \frac{r}{r_0} \right] \exp\left(-\frac{r^2}{r_0^2}\right) r dr}{\int_0^\infty \exp\left(-\frac{r^2}{r_0^2}\right) r dr} - \left[\frac{1}{2} \text{Ei} \left(-\frac{r_b^2}{r_0^2} \right) - \ln \frac{r_b}{r_0} \right] \right\} \\ &= \frac{1 - R - T}{2\pi k_{\text{eq}}t} C(r_0, r_b). \end{aligned} \quad (8)$$

The above analysis is based on the 1D approximation that temperature distributes uniformly in the cross-plane direction. To validate this assumption, we carried out 2D numerical heat transfer calculation with a source term that decays exponentially in the cross-plane direction to describe the actual laser absorption in the material and used the dimensionless quantity $\Delta T/(T_{\text{max}} - T_0)$ to evaluate the nonuniformity of the z -direction temperature distribution at $r = 0$, where ΔT is the temperature difference between the top and the bottom of the film, T_{max} is the maximum temperature in the entire film, and T_0 is the ambient temperature. We found that as film thickness increased to over 85 nm, the

dimensionless number became larger than 1% and we considered the cross-plane temperature distribution to be noticeably nonuniform. Therefore, for films thicker than 85 nm, a numerically solved 2D heat transfer model based on standard finite volume method was implemented instead of 1D analytical model.

RESULTS AND DISCUSSION

To obtain accurate temperature data from Raman spectra, careful calibrations were performed using a Linkam T95-HS heating stage (THMS720, Linkam, UK) for Bi films. The Raman laser power was controlled at the minimum level to avoid excessive sample heating while Raman scattering intensity was still strong enough to get accurate peak fitting. As seen in Figure 2a, The A_{1g} Raman peak of Bi at $\sim 97\text{ cm}^{-1}$ showed good temperature dependence. Figure 2b summarizes the calibration results of the A_{1g} peak. It is noted that for films thinner than 50 nm, the calibrated temperature coefficients were higher. This could be caused by microstructural changes for different film thicknesses or nonuniform cross-sectional strain in the film because the substrate is thin.

During experimental measurements of each Bi film, Raman spectra were taken under different laser powers. Raman peak shifts were then converted to temperature changes using the calibration coefficients. The measured temperature change varies with the laser power linearly as predicted by Eq. (8) (see the inset of Figure 3 as an example). Hence, the in-plane thermal conductivity of Bi films can be extracted by substituting the data slope into Eq. (8). The results are shown in Figure 3. It is noted that the sample temperature increased generally by $40\text{--}50^\circ\text{ K}$ at the laser irradiation center during the experiments; therefore, the thermal conductivity results are the thermal conductivities of the average temperature of the samples, which varies between 40 and 50° K above the room temperature at the center and the room temperature at the edge. The error bars are mostly attributed to the uncertainty of the slope of Raman-measured temperature vs. laser power (dT_{Raman}/dP), which accounts for $50\text{--}70\%$ of the total uncertainty in thermal conductivity; for those very thin films, the uncertainty of film thickness (typically $1\text{--}4\text{ nm}$) also accounts for about $30\text{--}40\%$ of the error. The other uncertainty sources, such as absorption and laser spot size, have been taken into account as well. One may note that in previously reported graphene thermal conductivity measurements using micro-Raman [20, 21], the total relative uncertainty

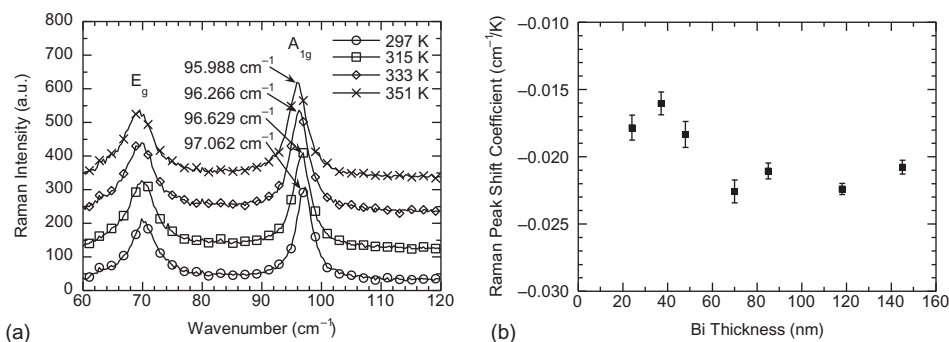


Figure 2 (a) Raman spectra taken under different temperatures during the calibration of 85-nm-thick Bi sample. Data are shifted vertically for a clearer view. The inset numbers denote the Lorentz fitted peak position of the A_{1g} Raman mode. (b) Calibration results of Raman peak shift vs. temperature.

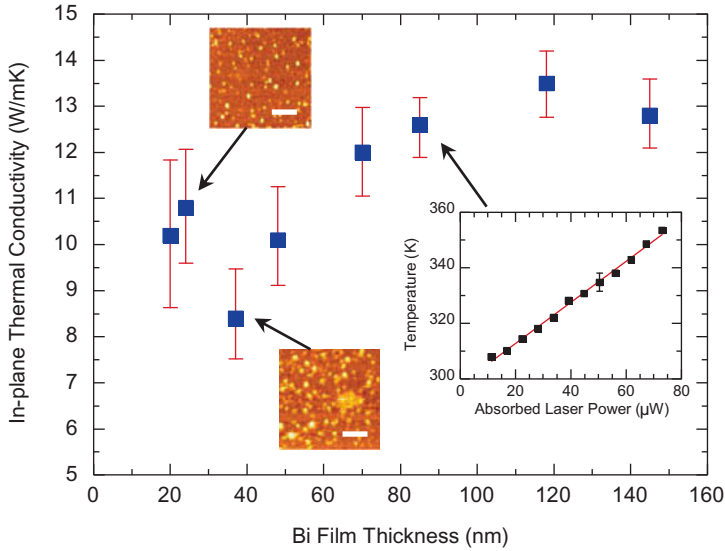


Figure 3 In-plane thermal conductivity of Bi films. The inset plots the measured temperature vs. absorbed laser power for the 85-nm film, and the black solid line is a linear fit. The inset pictures are atomic force microscope images of the 24- and 37-nm film surfaces, which show different surface feature densities. The scale bars are all 1 μm .

is relatively large, usually $\sim 30\%$ or higher, whereas in our work the uncertainty is less than 20%. This is mainly because the single-layer graphene absorbs only about 3% of the total laser power, yielding large relative uncertainties in the final results even with a very small uncertainty in determining the absorptivity. In contrast, our Bi films absorb 30–40% of the total incident power, which is much greater than that of graphene; therefore, the relative error of absorptivity is reduced, which gives more accurate in-plane thermal conductivity values.

At the nanoscale, it is known that the lattice thermal conductivity can be dramatically reduced as the characteristic length approaches the phonon mean free path (~ 150 nm for bulk Bi [23]). For films thicker than 100 nm, the measured in-plane thermal conductivity is in agreement with that of bulk Bi (~ 12 W/mK) reported by Gallo et al. [24], indicating that the film thickness and grain size are comparable to or larger than the phonon mean free path. As film thickness decreases, the in-plane thermal conductivity drops from about 12 W/mK to less than 9 W/mK. This reduction can be attributed to phonon boundary scattering at the film surface and interface, which restricts the phonon mean free path and subsequently reduces the lattice thermal conductivity. It is also possible that the grain size varies for different film thicknesses and further reduces the phonon mean free path. To take a closer look into grain boundary scattering, X-ray diffraction experiments were performed on these Bi samples using a Panalytical X'Pert Pro High Resolution X-ray diffraction (Panalytical Inc., MA, USA) system with Cu $K\alpha$ X-ray radiation of wavelength 1.54 \AA . The classic Scherrer equation [25] was used to estimate the sample grain size L :

$$L = \frac{K\lambda}{B \cos \theta}, \quad (9)$$

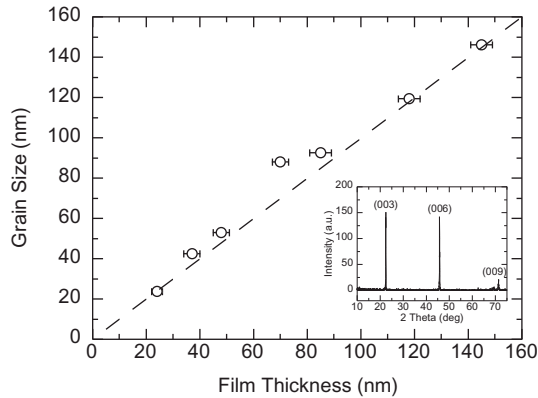


Figure 4 Grain sizes of Bi films calculated from the (003) peak of the X-ray diffraction data using Eq. (9). Grain size uncertainty is ~ 1 nm. The dashed line corresponds to where the grain size equals the film thickness. The inset shows a typical X-ray diffraction pattern. The angle step size is 0.02° .

where K is the Scherrer constant and is taken as 0.94, λ is the wavelength of the X-ray radiation, B is the full width at half maximum of the diffraction peak, and θ is the Bragg angle. Instrument broadening was considered to be minor due to small thickness and polycrystalline nature of the measured films, and the strain-induced broadening was likely to be constant for thermally evaporated Bi thicker than 20 nm [26], so the Scherrer equation is expected to give a good estimation of the grain size. From Figure 4 it is seen that the grain size is roughly equal to the film thickness, which indicates that in the thinner films the grain boundaries were more densely distributed in the lateral direction. In these Bi films, the atomic level disorders at the grain boundaries act as phonon scattering sites and therefore reduce the lattice in-plane thermal conductivity together with phonon surface/interface boundary scattering.

Surprisingly, an increase in the measured thermal conductivity is observed for films with thicknesses of about 20 nm. Two samples with similar thicknesses were used to verify this result. It was found that the surface asperities, which can scatter phonons, are probably responsible for the abnormal trend. As shown in the inset of Figure 3, the 24-nm Bi film has much less surface features than the 37-nm film. For the ~ 20 -nm films and other thicker films, the average number densities of asperities are 3.4 and $5\text{--}6 \mu\text{m}^{-2}$, respectively, and the average asperity sizes (full width at half maximum) are 117 and 160–230 nm, respectively. The relatively smaller number density and size of these surface features result in more specular and less diffusive phonon scattering at the sample surface for thinner Bi films; therefore, the thermal conductivity reduction effect due to diffusive phonon scattering is lower and causes higher in-plane thermal conductivity. The observed in-plane thermal conductivity increase for the ~ 20 -nm films may provide an insight into the roles of surface scattering and grain boundary scattering for reducing the in-plane thermal conductivity of Bi films. The measured in-plane thermal conductivity value of the ~ 20 -nm films, 11 W/mK, is close to those of the thickest Bi films measured in this work, $\sim 12\text{--}13$ W/mK. This means that grain boundary scattering contributes no more than 2 W/mK of the total thermal conductivity reduction, and the low thermal conductivity of the 37-nm film, ~ 8 W/mK, can be attributed to surface scattering. Therefore, surface scattering may have an equal or even larger role than grain boundary scattering in reducing the in-plane thermal conductivity of Bi films.

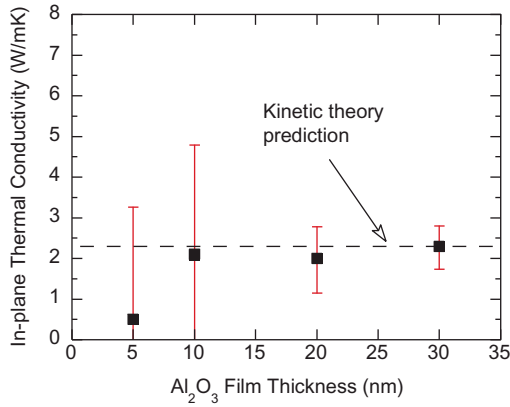


Figure 5 In-plane thermal conductivity of Al₂O₃ films. The dashed line corresponds to the kinetic theory prediction by Eq. (10) under the assumption that the phonon mean free path is restricted to be equal to the interatomic distance in amorphous solids.

We then used Bi film coated on Al₂O₃ film as a Raman temperature sensor to measure the in-plane thermal conductivity of Al₂O₃ films. Bi transducer film was deposited on Al₂O₃ instead of SiO₂ and therefore was calibrated separately and showed almost the same calibration result as Bi-SiO₂ samples of similar thicknesses (both are $-0.017 \text{ cm}^{-1}/\text{K}$). From Figure 5, the measured in-plane thermal conductivity values fall around 2 W/mK, consistent with the experimental results reported by Stark et al. [27] This value is much smaller than that of Al₂O₃ crystals (over 30 W/mK), which can be understood in the scope of minimum thermal conductivity model for dielectric crystals proposed by Slack [28]. In this model, a crystal is assumed to have strong intrinsic atomic-scale disorder that scatters the phonons frequently and consequently the phonon mean free path is limited to the interatomic distance, yielding the minimum thermal conductivity that can be reached in such disordered crystals. Because ALD-prepared Al₂O₃ films are in amorphous states, they resemble highly disordered Al₂O₃ and are expected to exhibit the predicted minimum thermal conductivity. A rough estimation can be carried out using the classic kinetic theory:

$$k = \frac{1}{3} C_v v l, \quad (10)$$

where C_v is the volumetric heat capacity, v is the average phonon group velocity, and l is the phonon mean free path and is taken as the equivalent interatomic spacing (the edge length of the average cubic space that is occupied by each atom) for the amorphous Al₂O₃ films. Taking $C_v = 3.1 \times 10^6 \text{ J/m}^3\text{K}$ [29], $v = 11 \text{ km/s}$ [30], $l = 2.04 \text{ \AA}$ [28], Eq. (10) indicates that the minimum thermal conductivity of Al₂O₃ is 2.3 W/mK, shown as a dashed line in Figure 5, which is in good agreement with the data. The minimum thermal conductivity model developed by Cahill et al. [31] gives a similar value of $\sim 1.8 \text{ W/mK}$ [32]. It is also seen that the measurement uncertainty is quite significant for 10- and 5-nm films. This is due to the reduction in the in-plane thermal conductance in the Al₂O₃ film as film thickness decreases. Because the Bi film used as the Raman temperature sensor has a much larger thermal conductivity ($\sim 10 \text{ W/mK}$) than the Al₂O₃ film (and the SiO₂ substrate), the steady-state temperature distribution becomes less sensitive to the Al₂O₃ thermal conductivity for very thin Al₂O₃ films, yielding relatively large uncertainties.

CONCLUSIONS

In this work, a micro-Raman-based optical method to measure in-plane thermal conductivity is presented and applied to Bi and Al_2O_3 thin films. The measured results of Bi films reveal that the phonon boundary scattering, both at the surface/interface and at grain boundaries, may be the cause of the reduction of the in-plane lattice thermal conductivity. The measurements of Al_2O_3 films were accomplished with the assist of Bi coatings as Raman temperature sensors, and the measured in-plane thermal conductivity results agree with proposed minimum thermal conductivity for dielectric solids. Our work demonstrates that the micro-Raman method is capable of measuring in-plane thermal conductivity of thin-film structures. In addition, a careful selection of the Raman temperature sensor material and the substrate material is necessary. The most desirable scenario is that the temperature sensor and substrate films have small thicknesses to assure 1D radial heat conduction, as well as low thermal conductivities to enhance heat flow through the sample film.

FUNDING

We acknowledge support from the DARPA MESO program (Grant N66001-11-1-4107). Y.F. is grateful for support from the Fundamental Research Funds for the Central Universities of China (FRF-AS-12-002, FRF-TP-11-001B).

REFERENCES

1. D.G. Cahill, Heat Transport in Dielectric Thin Films and at Solid–Solid Interfaces, *Microscale Thermophysical Engineering*, Vol. 1, pp. 85–109, 1997.
2. K.E. Goodson and Y.S. Ju, Heat Conduction in Novel Electronic Films, *Annual Review of Materials Science*, Vol. 29, pp. 261–293, 1999.
3. R. Venkatasubramanian, E. Siivola, T. Colpitts, and B. O’Quinn, Thin-Film Thermoelectric Devices with High Room-Temperature Figures of Merit, *Nature*, Vol. 413, pp. 597–602, 2001.
4. G. Chen, M.S. Dresselhaus, G. Dresselhaus, J.P. Fleurial, and T. Caillat, Recent Developments in Thermoelectric Materials, *International Materials Reviews*, Vol. 48, pp. 45–66, 2003.
5. H. Böttner, G. Chen, and R. Venkatasubramanian, Aspects of Thin-Film Superlattice Thermoelectric Materials, Devices, and Applications, *MRS Bulletin*, Vol. 31, pp. 211–217, 2006.
6. A. Shakouri, Recent Developments in Semiconductor Thermoelectric Physics and Materials, *Annual Review of Materials Research*, Vol. 41, pp. 399–431, 2011.
7. G. Chen, Size and Interface Effects on Thermal Conductivity of Superlattices and Periodic Thin-Film Structures, *Journal of Heat Transfer*, Vol. 119, pp. 220–229, 1997.
8. G. Chen, Thermal Conductivity and Ballistic-Phonon Transport in the Cross-Plane Direction of Superlattices, *Physical Review B*, Vol. 57, pp. 14958–14973, 1998.
9. D.G. Cahill, Thermal Conductivity Measurement from 30–750 K: The 3ω Method, *Review of Scientific Instruments*, Vol. 61, pp. 802–808, 1990.
10. S.M. Lee and D.G. Cahill, Heat Transport in Thin Dielectric Films, *Journal of Applied Physics*, Vol. 81, pp. 2590–2595, 1997.
11. R. Venkatasubramanian, Lattice Thermal Conductivity Reduction and Phonon Localizationlike Behavior in Superlattice Structures, *Physical Review B*, Vol. 61, pp. 3091–3097, 2000.
12. Z. Li, S. Tan, E. Bozorg-Grayeli, T. Kodama, M. Asheghi, G. Delgado, M. Panzer, A. Pokrovsky, D. Wack, and K.E. Goodson, Phonon Dominated Heat Conduction Normal to Mo/Si Multilayers with Period below 10 nm, *Nano Letters*, Vol. 12, pp. 3121–3126, 2012.

13. W.S. Capinski, H.J. Maris, T. Ruf, M. Cardona, K. Ploog, and D.S. Katzer, Thermal-Conductivity Measurements of GaAs/AlAs Superlattices Using a Picosecond Optical Pump-and-Probe Technique, *Physical Review B*, Vol. 59, pp. 8105–8113, 1999.
14. D. Chu, M. Touzelbaev, K.E. Goodson, S. Babin, and R.F. Pease, Thermal Conductivity Measurements of Thin-Film Resist, *Journal of Vacuum Science & Technology B*, Vol. 19, pp. 2874–2877, 2001.
15. Y.K. Koh, C.J. Vineis, S.D. Calawa, M.P. Walsh, and D.G. Cahill, Lattice Thermal Conductivity of Nanostructured Thermoelectric Materials Based on PbTe, *Applied Physics Letters*, Vol. 94, pp. 153101, 2009.
16. F. Völklein, H. Reith, and A. Meier, Measuring Methods for the Investigation of In-Plane and Cross-Plane Thermal Conductivity of Thin Films, *Physica Status Solidi A*, Vol. 210, pp. 106–118, 2013.
17. A. Mavrokefalos, N.T. Nguyen, M.T. Pettes, D.C. Johnson, and L. Shi, In-Plane Thermal Conductivity of Disordered Layered WSe₂ and (W)_x(WSe₂)_y Superlattice Films, *Applied Physics Letters*, Vol. 91, pp. 171912, 2007.
18. A.A. Balandin, S. Ghosh, W. Bao, I. Calizo, D. Teweldebrhan, F. Miao, and C.N. Lau, Superior Thermal Conductivity of Single-Layer Graphene, *Nano Letters*, Vol. 8, pp. 902–907, 2008.
19. C. Faugeras, B. Faugeras, M. Orlita, M. Potemski, R.R. Nair, and A.K. Geim, Thermal Conductivity of Graphene in Corbino Membrane Geometry, *ACS Nano*, Vol. 4, pp. 1889–1892, 2010.
20. W. Cai, A.L. Moore, Y. Zhu, X. Li, S. Chen, L. Shi, and R.S. Ruoff, Thermal Transport in Suspended and Supported Monolayer Graphene Grown by Chemical Vapor Deposition, *Nano Letters*, Vol. 10, pp. 1645–1651, 2010.
21. J.U. Lee, D. Yoon, H. Kim, S.W. Lee, and H. Cheong, Thermal Conductivity of Suspended Pristine Graphene Measured by Raman Spectroscopy, *Physical Review B*, Vol. 83, pp. 081419, 2011.
22. Y.S. Touloukian, R.W. Powell, C.Y. Ho, and P.G. Klemens, *Thermal Conductivity*, TPRC Data Series, Vol. 2, Plenum, New York, 1970.
23. A.L. Moore, M.T. Pettes, F. Zhou, and L. Shi, Thermal Conductivity Suppression in Bismuth Nanowires, *Journal of Applied Physics*, Vol. 106, p. 034310, 2009.
24. C.F. Gallo, B.S. Chandrasekhar, and P.H. Sutter, Transport Properties of Bismuth Single Crystals, *Journal of Applied Physics*, Vol. 34, pp. 144–152, 1963.
25. J.I. Langford and A.J.C. Wilson, Scherrer after Sixty Years: A Survey and Some New Results in the Determination of Crystallite Size, *Journal of Applied Crystallography*, Vol. 11, pp. 102–113, 1978.
26. A.A. Ramadan, A.M. El-Shabiny, and N.Z. El-Sayed, Size-Dependent Structural Characteristics of Thin Bismuth Films, *Thin Solid Films*, Vol. 209, pp. 32–37, 1992.
27. I. Stark, M. Stordeur, and F. Syrowatka, Thermal Conductivity of Thin Amorphous Alumina Films, *Thin Solid Films*, Vol. 226, pp. 185–190, 1993.
28. G.A. Slack, The Thermal Conductivity of Nonmetallic Crystals, in eds. F. Seitz and D. Turnbull, *Solid State Physics*, Vol. 34, pp. 1–71, Academic, New York, 1979.
29. D.A. Ditmars, S. Ishihara, S.S. Chang, G. Bernstein, and E.D. West, Enthalpy and Heat-Capacity Standard Reference Material: Synthetic Sapphire (α -Al₂O₃) from 10 to 2250 K, *Journal of Research of the National Bureau of Standards*, Vol. 87, pp. 159–163, 1982.
30. J.M. Winey, Y.M. Gupta, and D.E. Hare, R-Axis Sound Speed and Elastic Properties of Sapphire Single Crystals, *Journal of Applied Physics*, Vol. 90, pp. 3109–3111, 2001.
31. D.G. Cahill, S.K. Watson, and R.O. Pohl, Lower Limit to the Thermal Conductivity of Disordered Crystals, *Physical Review B*, Vol. 46, pp. 6131–6140, 1992.
32. S.M. Lee and D.G. Cahill, Thermal Conductivity of Sputtered Oxide Films, *Physical Review B*, Vol. 52, pp. 253–257, 1995.